AIP Journal of Applied Physics

Long-term stability of a quasiperiodic Ta/Al multilayer: Disintegration at room temperature analyzed by grazing angle x-ray scattering and photoelectron spectroscopy

P. Yang, U. Klemradt, Y. Tao, J. Peisl, R. W. Peng, A. Hu, and S. S. Jiang

Citation: Journal of Applied Physics **86**, 267 (1999); doi: 10.1063/1.370725
View online: http://dx.doi.org/10.1063/1.370725
View Table of Contents: http://scitation.aip.org/content/aip/journal/jap/86/1?ver=pdfcov
Published by the AIP Publishing

Articles you may be interested in

Evolution of nanoscale roughness in Cu/SiO2 and Cu/Ta interfaces
Appl. Phys. Lett. **100**, 024106 (2012); 10.1063/1.3675611

Influence of nanocrystal growth kinetics on interface roughness in nickel–aluminum multilayers
Appl. Phys. Lett. **83**, 5437 (2003); 10.1063/1.1637155

Nonspecular x-ray reflectivity study of roughness scaling in Si/Mo multilayers
J. Appl. Phys. **89**, 1101 (2001); 10.1063/1.1332095

Thermal stability of 2.4 nm period Ni–Nb/C multilayer x-ray mirror
Appl. Phys. Lett. **77**, 3654 (2000); 10.1063/1.1328761

Thermal stability of Cu/Ta/GaAs multilayers
Appl. Phys. Lett. **77**, 3367 (2000); 10.1063/1.1328094

[This article is copyrighted as indicated in the article. Reuse of AIP content is subject to the terms at: http://scitation.aip.org/termsconditions. Downloaded to] IP: 202.119.48.169 On: Wed, 22 Apr 2015 12:22:17

Long-term stability of a quasiperiodic Ta/Al multilayer: Disintegration at room temperature analyzed by grazing angle x-ray scattering and photoelectron spectroscopy

P. Yang[a] and U. Klemradt[b]
Sektion Physik der Ludwig-Maximilians-Universität München, Geschwister-Scholl-Platz 1, D-80539 München, Germany

Y. Tao
Institute for Microstructural Sciences, National Research Council, Ottawa K1A OR9, Canada

J. Peisl
Sektion Physik der Ludwig-Maximilians-Universität München, Geschwister-Scholl-Platz 1, D-80539 München, Germany

R. W. Peng, A. Hu, and S. S. Jiang
Laboratory of Solid State Microstructures, Nanjing University, Nanjing 210008, People's Republic of China

(Received 1 July 1998; accepted for publication 1 March 1999)

A three-component Fibonacci (3CF) Ta/Al multilayer has been reinvestigated by specular and diffuse x-ray reflectivity and x-ray photoelectron spectroscopy (XPS) after 41 months of storage at room temperature. The specular reflectivity shows drastically suppressed diffraction peaks, whose positions and intensities are explained by severe interdiffusion of the Ta/Al bilayers building the 3CF sequence. Nonspecular reflectivity scans still indicate a high degree of interfacial roughness correlation in the growth direction that is attributed to the long spatial Fourier components of the interface profiles, which are substantially less affected by interdiffusion. The angle-resolved XPS spectra show that the Ta capping layer is completely oxidized and interdiffused by Al, whereas below the oxide layer Ta and Al coexist in metallic form in the same film. Both x-ray reflectivity and XPS yield an oxide layer of ~30 Å thickness. Despite the severe structural disintegration, the multilayer diffraction spectrum can still be indexed by means of the projection theory for quasiperiodic sequences, which points to a remarkable stability of quasiperiodic properties against significant disorder. We conclude that Ta/Al bilayers are apparently unsuitable for multilayer applications due to the lack of thermal stability even at room temperature, with grain boundary diffusion pointed out as a possible disintegration mechanism. The design of improved 3CF Ta/Al multilayers is discussed with regard to applications in x-ray optics. © *1999 American Institute of Physics.* [S0021-8979(99)02212-4]

I. INTRODUCTION

Artificial multilayers have attracted much attention over the past 2 decades because of the many unusual physical properties exhibited by these new materials, which in turn have fostered important applications ranging from electronic devices to x-ray monochromators.[1–3] Although many material combinations have been considered in the literature for each functional use, most practical devices are based on a rather limited number of materials that represent well-established compromises between device performance, deposition requirements, long-term stability, etc. Especially the last aspect is very important when multilayers are produced from new material combinations, which—if prone to degradation—give rise to poor device characteristics in the long run despite promising initial results. It has been realized that particularly multilayers based on thin films with sharp interfaces can exhibit unexpected structural changes e.g., amorphization if sufficient additional interfacial free energy is present in a multilayer of a given thickness,[4] or homogenization due to enhanced interdiffusion resulting from strong compositional gradients.[5,6]

In recent years Ta has been increasingly used as a multilayer material. Whereas Ta/Fe- and Ta/Ni-based multilayers[7–9] have attracted attention on account of their magnetic properties, Ta/Nb and Ta/Al layered structures have been investigated with regard to applications in superconductivity[10] and advanced x-ray instrumentation. In particular, Nb/Ta/Al films were shown to be efficient x-ray detectors,[11] and periodic as well as quasiperiodic Ta/Al multilayers were studied owing to their potential as x-ray monochromators.[12–17] Compared to a frequently used combination like W/C, the pair Ta/Al offers advantages for the fabrication of reflecting and dispersing optical elements in the x-ray regime. High peak reflectivities are still obtained due to the large electron density contrast, but are less affected by absorption from the heavy element since the linear absorption coefficient μ is significantly larger for W than for

[a]Present address: School of Physics, Universiti Sains Malaysia, USM 11800 Penang, Malaysia.
[b]Author to whom correspondence should be addressed; electronic mail: uwe.klemradt@physik.uni-muenchen.de

 © 1999 American Institute of Physics
[This article is copyrighted as indicated in the article. Reuse of AIP content is subject to the terms at: http://scitation.aip.org/termsconditions. Downloaded to] IP: 202.119.48.169 On: Wed, 22 Apr 2015 12:22:17

Ta (20.5% at Cu K_α radiation); in addition, the deposition of pure Al instead of the carbon commonly used for this purpose can also be economically more favorable.[15] However, such multilayers need to be stable over an extended period of use.

In this article we report the structural analysis of a three-component Fibonacci (3CF) Ta/Al multilayer after extensive aging at room temperature. The results of the initial characterization shortly after growth have been published elsewhere[16] and will not be repeated here in detail. The present investigation aims at two different aspects of stability in 3CF Ta/Al multilayers: First, the long-term material properties of Ta/Al multilayers—initially produced with excellent layer and interface quality—are assessed by a detailed structural investigation using specular and nonspecular x-ray reflectivity and photoelectron spectroscopy. Second, the effect of degradation-induced disorder on the quasiperiodic diffraction spectrum is studied since particularly 3CF multilayers have been suggested as x-ray monochromators (cf. Sec. II).

II. 3CF QUASIPERIODIC MULTILAYER DESIGN

Multilayers fabricated by *quasiperiodic* deposition sequences of thin films constitute an important and very interesting class of layered structures, which—although perfectly ordered by construction—represent an intermediate case between periodic and random systems due to the absence of translational invariance. Fibonacci lattices appear to be the most frequently studied type of one-dimensional (1D) deterministic, nonperiodic sequences. Their unique electronic structure and transport properties have been established both theoretically and experimentally,[18] and the discovery of quasicrystals has stimulated much work on the physical properties of quasiperiodic multilayers as these are the 1D analogs of quasicrystals.[19]

Multilayers have been applied in x-ray optics for more than a decade, and periodic structures based on alternating layers of high-Z/low-Z elements have proved very efficient as high-flux monochromators and reflectors for soft x-rays under nearly normal incidence as well as for hard x-rays under grazing angles.[3,20] Quasiperiodic multilayers are very interesting as x-ray optical devices mainly for two reasons: They give rise to an aperiodic diffraction pattern (reflecting the self-similarity of the underlying sequence of layers), which can be used for the efficient suppression of higher harmonics contaminating a monochromatized beam, since the scattering vectors of these higher harmonics will—in general—not coincide with the position of diffraction peaks. Furthermore, the long-range order of the quasiperiodic stacking sequence can result in strong (or even the strongest) reflectivity peaks at relatively large incident angles of more than 1° for x-ray wavelengths around 1.5 Å. Therefore such multilayers can be used as normal-incidence reflectors for soft x-rays at relatively high energies (≈800–1000 eV), where the use of periodic structures would require a d spacing of $\lambda/2$ that is difficult to produce since it approaches interatomic distances.[14]

1D aperiodic sequences can be generated by the repeated application of substitution rules. An important example for quasiperiodic sequences of two building blocks is $A \rightarrow A^m B, B \rightarrow A$, where m is an integer. This rule gives the classic Fibonacci sequence as a special case for $m=1$. A few non-Fibonacci structures have been studied experimentally, including the case $m \neq 1$ for the above rule[21] and Thue–Morse sequences,[22] which are based on the inflation rule $A \rightarrow AB, B \rightarrow BA$. *Nonstandard* 1D Fibonacci sequences can be generated by using more than two building blocks.[16] It has been shown that only structures with $2 \leqslant k \leqslant 5$ components are quasiperiodic and hence can be treated as the projection of a high-dimensional periodic lattice, which in turn leads to a k-dimensional indexing of the x-ray diffraction spectrum from k-component structures.[23] The theory was tested for three-component Fibonacci multilayers, and the measured peak positions were found to be in good agreement with theoretical values based on 3D indexing.[16,17] Multicomponent Fibonacci multilayers are especially attractive for x-ray optical applications since they offer more flexibility than two-component structures to tailor the diffraction pattern to specific needs; in particular, this might be used to reduce the overall absorption of the multilayer by optimizing the relative thickness of high-Z layers.

The generalized Fibonacci sequence for $k=3$ elements can be generated by the recursion formula

$$a_r = a_{r-1} + a_{r-3} \tag{1}$$

from three seeds $a_1 = a_2 = 0$, $a_3 = 1$.[23] A corresponding 3CF multilayer is based on three building blocks A, B and C (which are bilayers with thicknesses d_A, d_B, and d_C, respectively), and the layer sequence S_r of a sample consisting of r Fibonacci generations is constructed consequently as $S_r = S_{r-1} \oplus S_{r-3}$, with $S_1 = \{A\}$, $S_2 = \{AC\}$, and $S_3 = \{ACB\}$. This gives rise to the chain $A \rightarrow AC \rightarrow ACB \rightarrow ACBA \rightarrow ACBAAC \rightarrow ACBAACACB \ldots$, so that the infinite Fibonacci series contains all its finite truncations and is therefore self-similar and spatially quasiperiodic. Alternatively, the 3CF sequence can be generated by the inflation rule $A \rightarrow AC, C \rightarrow B, B \rightarrow A$, which can be expressed conveniently using a 3×3 matrix:

$$\begin{pmatrix} A \\ B \\ C \end{pmatrix} \rightarrow \mathbf{M} \begin{pmatrix} A \\ B \\ C \end{pmatrix} \quad \text{with} \quad \mathbf{M} = \begin{bmatrix} 1 & 0 & 1 \\ 1 & 0 & 0 \\ 0 & 1 & 0 \end{bmatrix}. \tag{2}$$

For an infinite series, the ratio of building blocks is given by $\xi = \lim_{r \rightarrow \infty} [N_r(B)/N_r(A)]$ and $\eta = \lim_{r \rightarrow \infty} [N_r(C)/N_r(A)]$, where $N_r(X)$ denotes the number of building blocks X in a finite realization S_r of the 3CF series. According to the inflation rule, ξ and η can be determined from the following equations:

$$\eta + \eta^3 = 1, \tag{3}$$

$$\xi = \eta^2, \tag{4}$$

which yield $\xi = 0.46557...$ and $\eta = 0.68233...$. It should be noted that Eq. (3) can be derived directly from the matrix $\mathbf{M}$, since $1/\eta$ is the only real root of its characteristic polynomial $\lambda^3 - \lambda^2 - 1 = 0$.[16] The above theory was used to devise a 3CF multilayer based on Ta/Al bilayers. Figure 1 depicts a schematic drawing of the sample structure. Each bilayer con-

[This article is copyrighted as indicated in the article. Reuse of AIP content is subject to the terms at: http://scitation.aip.org/termsconditions. Downloaded to] IP: 202.119.48.169 On: Wed, 22 Apr 2015 12:22:17

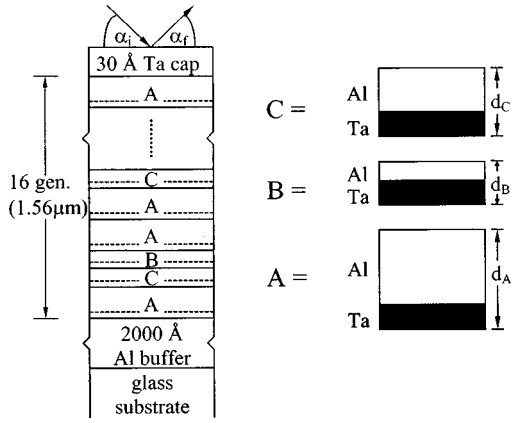

FIG. 1. Sketch of the three-component Fibonacci (3CF) Ta/Al multilayer sample with building blocks *A* (36.4 Å Al/12.7 Å Ta), *B* (9.9 Å Al/12.7 Å Ta), and *C* (21.1 Å Al/12.7 Å Ta). The angles α_i and α_f are greatly exaggerated and refer to the incident and scattered x-rays, respectively.

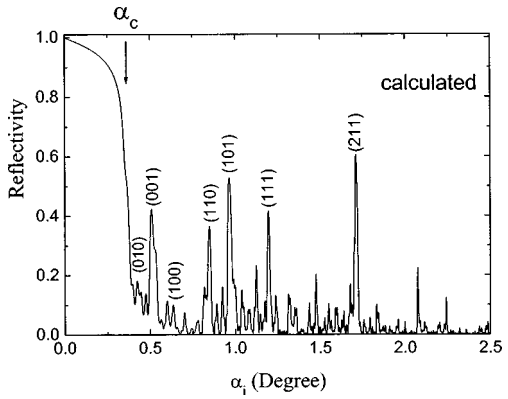

FIG. 2. Calculated specular reflectivity for the sample structure from Fig. 1 ($\lambda = 1.54$ Å).

sisted of an Al film on top of a 12.7 Å Ta film. The total thicknesses of the building blocks were $d_A = 49.1$ Å, $d_B = 22.6$ Å, and $d_C = 33.8$ Å, which gave ratios d_B/d_A and d_C/d_A very close to ξ and η, respectively. The 3CF series was truncated after 16 generations and resulted in a multilayer of ~1.56 μm thickness, containing 189 bilayers of type *A*, 88 of type *B*, and 129 of type *C*. A Ta cap layer of about 30 Å was grown in addition to the Fibonacci sequence. The sample was fabricated on a glass substrate by dual-target magnetron sputtering. A more detailed description of the sample preparation can be found in Ref. 16.

III. DIFFRACTION PROPERTIES OF 3CF MULTILAYERS

The low-angle x-ray diffraction spectrum of multilayers can be calculated accurately by classical optics, taking into account explicitly absorption and multiple scattering. Therefore this approach describes also the total reflection part of the specular reflectivity, which allows us to scale the diffraction peak heights to the incident intensity. The calculations are based on Fresnel's equations for the appropriate index of refraction for each layer, which is given for hard x-rays by[24]

$$n = 1 - \delta$$

with

$$\delta = \frac{r_0}{2\pi}\lambda^2 \rho_e, \tag{5}$$

where $r_0 = 2.818 \times 10^{-15}$ m is the classical electron radius, λ denotes the x-ray wavelength, and ρ_e is the electron density of the layer. As n is less than unity, total external reflection occurs for x-rays incident below a critical angle $\alpha_C = \sqrt{2\delta}$, which is typically a few tenths of a degree. Our numerical simulations were based on a Parratt algorithm[25] in the form used by Stanglmeier *et al.*,[26] which treats properly the electromagnetic boundary conditions at all interfaces and includes dispersion and absorption corrections. Interface roughness was modeled according to Névot and Croce.[27]

Figure 2 shows the calculated specular reflectivity at $\lambda = 1.54$ Å for the 3CF multilayer from Fig. 1, assuming interfaces with zero roughness. The critical angle, given by $\alpha_C = \sqrt{2\bar{\delta}} \approx 0.35°$, is smeared out due to the strong absorption of Ta layers. Since the capping layer is relatively thin, the evanescent x-ray wave probes parts of the multilayer, and therefore the refractive properties are best described by a thickness-weighted average $\bar{\delta} = 1.87 \times 10^{-5}$, instead of calculating δ only from the capping layer material. Evidently, the diffraction pattern of a 3CF multilayer differs significantly from that of a periodic superlattice, and it should be noted that the theoretical peak reflectivities exceed 50% for this structure, with the highest reflectivity at a very large incident angle $\alpha_i = 1.71°$ (cf. Sec. II).

Indexing can be done by the projection method, using the Fourier transform of the high-dimensional lattice related to the quasiperiodic ordering in real space. Due to the three-component multilayer structure, the diffraction pattern must be indexed by three numbers n_1, n_2, n_3. The scattering vectors of the strong peaks are given by this method as[16]

$$q(n_1, n_2, n_3) = \frac{2\pi}{D}(n_1 + n_2\xi + n_3\eta), \tag{6}$$

with the average lattice parameter

$$D = d_A + d_B\xi + d_C\eta. \tag{7}$$

The self-similarity of the diffraction pattern is expressed by the recursion relation

$$q(a_n, a_{n-2}, a_{n-1}) = q(a_{n-1}, a_{n-3}, a_{n-2}) + q(a_{n-3}, a_{n-5}, a_{n-4}), \tag{8}$$

which can be regarded as the Fourier transform analog of the relation $S_r = S_{r-1} \oplus S_{r-3}$, which defines the 3CF layer sequence in real space. The indexes a_n are the generalized Fibonacci numbers specified in Eq. (1).

Table I lists the peak positions and reflectivities from our simulation. The assigned indexing can be checked using Eqs. (6) and (8), since the scattering vectors q are defined relative to *any* Bragg peak of the underlying material, which includes also extreme forward scattering like specular reflectivity under grazing angles, which is not sensitive to crystallinity at all. However, refraction corrections are essential to account for peak positions close to the total reflection regime. They can be performed easily by replacing the x-ray wavelength λ

[This article is copyrighted as indicated in the article. Reuse of AIP content is subject to the terms at: http://scitation.aip.org/termsconditions. Downloaded to] IP: 202.119.48.169 On: Wed, 22 Apr 2015 12:22:17

TABLE I. Calculated reflection data for a perfect 3CF Ta/Al multilayer with $D=82.7$ Å and $\lambda=1.54$ Å. The reflectivity is scaled to the incident intensity I_0. The scattering vectors are defined as $q_{\text{uncorr}}=4\pi/\lambda \sin\alpha_i$ (no refraction correction), $q_{\text{corr}}=4\pi/\lambda \sin\alpha_i\sqrt{1-2\overline{\delta}/\sin^2\alpha_i}$ (refraction correction with $\overline{\delta}=1.87\times10^{-5}$), and $q_{\text{theor}}=2\pi/D(n_1+n_2\xi+n_3\eta)$.

Index (n_1,n_2,n_3)	Incident angle α_i (deg)	Reflectivity (I/I_0)	q_{uncorr} (Å^{-1})	q_{corr} (Å^{-1})	q_{theor} (Å^{-1})
(010)	0.424	0.18	0.0604	0.0340	0.0354
(001)	0.510	0.42	0.0726	0.0528	0.0518
(100)	0.635	0.10	0.0904	0.0754	0.0760
(110)	0.850	0.37	0.121	0.110	0.111
(101)	0.965	0.53	0.137	0.128	0.128
(111)	1.197	0.42	0.170	0.163	0.163
(211)	1.710	0.61	0.243	0.238	0.239

and the incident angle α_i in vacuum (or air) by the corresponding values inside the medium. Using Snell's law $\cos\alpha_i=n_M\cos\alpha_M$ and neglecting higher orders in δ, we obtain for the corrected scattering vectors

$$q_{\text{corr}}=\frac{4\pi}{\lambda}\sin\alpha_i\sqrt{1-2\overline{\delta}/\sin^2\alpha_i}. \tag{9}$$

The corrected scattering vectors are also listed in Table I and compare well with the peak positions derived from Eq. (6). The small deviations for very shallow incident angles reflect that a fixed average value for $\overline{\delta}$ is only a first approximation, since the x-ray penetration depth increases with the angle of incidence. We note that the recursion relation, Eq. (8), is also satisfied, e.g., $q(2,1,1)=q(1,1,1)+q(1,0,0)$.

IV. EXPERIMENTAL RESULTS

The sample was characterized shortly after growth by high- and low-angle x-ray diffraction using a low resolution powder diffractometer.[16] Both data sets confirmed the quasiperiodicity of the multilayer. The high-angle data showed that the layers were mainly crystalline with a texture dominated by Ta(110) and Al(111). The low-angle diffraction data correspond essentially to the reflectivity measurements performed here, although neither the total reflection regime nor off-specular scattering had been recorded. In this work, the sample was reinvestigated after 41 months of storage at room temperature by high resolution x-ray reflectivity and x-ray photoelectron spectroscopy (XPS).

X-ray reflectivity measurements were performed with a Rigaku rotating anode generator running at 21 kW and equipped with a Ge(111) channel-cut monochromator to select Cu $K_{\alpha1}$ radiation. The incident x-ray beam was 4 mm high and 0.1 mm wide with a divergence of $\sim0.007°$ in the scattering plane. The detector slit was at a distance of 315 mm from the sample and opened 0.15 mm in order to receive the entire specular beam while minimizing the pickup of background scattering. For intensity reasons, the same slit settings were also used in nonspecular reflectivity (diffuse scattering) measurements. Specular and diffuse reflectivities were scanned in 0.005° and 0.010° steps, respectively.

Since rough multilayer interfaces can lead to pronounced diffuse scattering under grazing angles, it was important to eliminate this background from the measured specular data

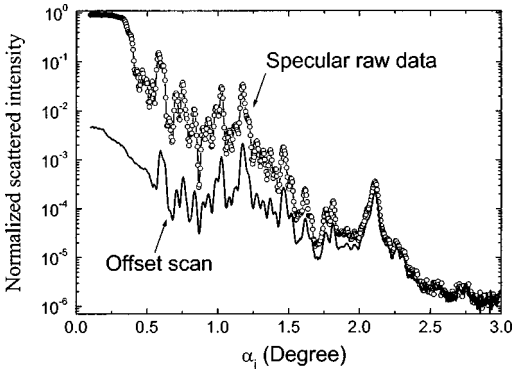

FIG. 3. Measured intensity under specular ($\alpha_f=\alpha_i$) and non-specular ($\alpha_f=\alpha_i-0.15°$) conditions. The offset scan indicates a strong correlation of interfacial roughness in growth direction.

to establish the specular reflectivity. This was accomplished by two offset scans with $\alpha_f=\alpha_i\pm0.15°$, which were averaged and subtracted from the specular raw data. The slightly detuned specular condition ensured that only diffuse scattering in the vicinity of the specular path was recorded. Figure 3 shows the specular raw data and an offset scan, indicating that diffuse scattering contributes significantly to the specular intensity already at $\alpha_i=1.25°$ and dominates the signal above $\alpha_i=2.5°$. It should be noted that the diffuse scattering varies considerably with the angle of incidence since it mimics the specular curve, which is strong evidence for a high degree of interfacial roughness correlation.[28]

The logarithmic intensity scale necessary for Fig. 3 points to major deviations from the ideal diffraction pattern shown in Fig. 2. However, the experimental data can be explained remarkably well on the basis of a 3CF structure if we allow for severe interdiffusion of the multilayer building blocks. To restrict the number of fit parameters for this 813 layer system, we assumed that all building blocks of a given type could be described by the same parameters for thickness, density, and interface roughness. Different stages of interdiffusion, depicted in Fig. 4, were tested by numerical simulation for their ability to account for the experimental specular curve. It turned out that the data could only be fitted by a model of severe interdiffusion, corresponding to stage 3 for the thick building block *A* and stage 4 for the thin building blocks *B* and *C*. In other words, the simulations suggest that completely interdiffused layers constitute the blocks *B* and *C*, whereas block *A* consists of a remaining Al layer sandwiched between interdiffusion layers. Figure 5 shows a fit to the specular reflectivity based on this model with fit

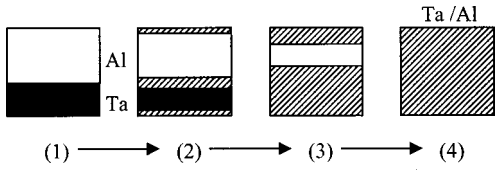

FIG. 4. Progressive stages of bilayer interdiffusion from non-interdiffused (1) to completely interdiffused (4) used for modeling the real structure of the multilayer building blocks.

[This article is copyrighted as indicated in the article. Reuse of AIP content is subject to the terms at: http://scitation.aip.org/termsconditions. Downloaded to] IP: 202.119.48.169 On: Wed, 22 Apr 2015 12:22:17

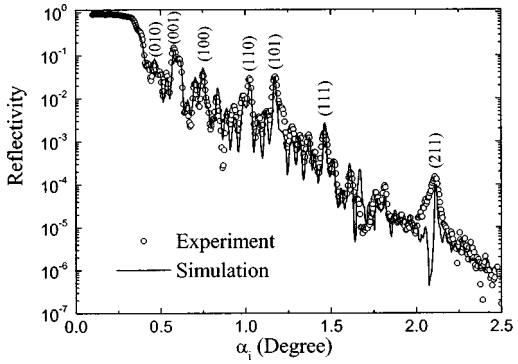

FIG. 5. Background-corrected specular reflectivity (circles) and fit (line) based on a model of severe interdiffusion of the multilayer building blocks.

parameters listed in Table II. The goodness of the fit is quantified by an R factor of 4.34%, with R defined as

$$R=\frac{\Sigma_i|Y_i^c-Y_i^o|}{\Sigma_i Y_i^o}. \tag{10}$$

The simulation yields a very light oxide layer, indicating that the original Ta capping layer has been completely oxidized and interdiffused, consistent with the XPS results discussed below. The fit is essentially insensitive to the surface roughness, which is not surprising here since this parameter corresponds to the electron density smearing between the vacuum and a layer of very low electron density. The interdiffusion layers in all building blocks have been treated identically, which is somewhat oversimplified but allowed us to use an elementary structural model with only eight fit parameters, since there is no meaningful interface roughness between identical layers. The ratio of Ta to Al atoms was approximated as 1:1 within the interdiffusion layers, reflecting the comparable number densities of Ta and Al atoms in the originally deposited layers.[29] The interface roughness of 8 Å between the remaining Al slab in block *A* and the adjacent interdiffusion layers is relatively large for a slab of 15 Å thickness, which indicates a graded index of refraction that is presumably due to interdiffusion progressing from stage 3 to stage 4.

The observed specular intensities and peak positions are listed in Table III together with the corresponding 3CF indexes according to Eqs. (6) and (7). Since the average lattice parameter D depends sensitively on the individual parameters for d_A, d_B, and d_C because of the weights ξ and η, the comparison of experimental and theoretical peak positions in Table III confirms directly and in detail the ability of our modified 3CF structural model to account for the measured data, in addition to the overall goodness of the fit.

The question might arise if indexing in terms of a *three*-component Fibonacci structure is on firm grounds here since the building blocks *B* and *C* are indistinguishable except for their thicknesses. However, although *C* is mostly followed by *B*, the distinction between these building blocks is not artificial because the 3CF sequence contains isolated building blocks of type *C* as well.

The chemical state of the surface was analyzed by XPS measurements, which were performed in a Perkin–Elmer PHI-5500 system equipped with a monochromated Al K_α source. High resolution Al $2p$ and Ta $4f$ core level data were collected at a pass energy of 5.85 eV. Figure 6 shows Ta $4f$ spectra taken at different take-off angles (defined as the angle between the electron energy analyzer and the sample surface) to obtain chemical information at different depths. The main features of Fig. 6 are two peak doublets arising from spin splitting into $4f_{5/2}$ and $4f_{7/2}$ states in different chemical environments. The doublet at lower binding energies (when counted positive) stems from metallic Ta, whereas the doublet at higher energies corresponds to the

TABLE II. Structural parameters of the 3CF multilayer after 41 months at room temperature, determined by a fit to the x-ray reflectivity (Fig. 5). Fit parameters are indicated by error bounds.

Layer	Thickness (Å)	Density (g/cm^3)	Roughness (Å)
Capping layer	26±10	2±1	n.a.
Building block *A*:			
Interdiffusion layers	25.0±0.5	9.1±0.3	—
Al layer	15.0±0.5	2.7	8±1
Building block *B*:			
Interdiffusion layer	17.0±0.5	9.1±0.3	—
Building block *C*:			
Interdiffusion layer	27.4±0.5	9.1±0.3	—

TABLE III. Experimental reflection data for the 3CF Ta/Al multilayer ($\lambda=1.54$ Å) and 3CF indexing based on the average lattice parameter $D=66.6$ Å obtained from the fit. Values for q_{corr} were calculated with a modified refraction correction $\bar{\delta}=1.93\times10^{-5}$ to account for layer interdiffusion (for symbol definitions see Table I).

Index (n_1,n_2,n_3)	Incident angle α_i (deg)	Specular intensity (I/I_0)	q_{corr} (Å^{-1})	q_{theor} (Å^{-1})
(1 0 −1)	0.425	6.75×10^{-2}	0.0331	0.0300
(0 1 0)	0.465	6.69×10^{-2}	0.0426	0.0439
(1 −1 0)	0.495	4.26×10^{-2}	0.0490	0.0504
(−1 2 1)	0.535	4.00×10^{-2}	0.0569	0.0579
(0 0 1)	0.580	1.53×10^{-1}	0.0652	0.0644
(1 1 −1)	0.620	8.62×10^{-2}	0.0723	0.0739
(−1 1 2)	0.650	6.91×10^{-3}	0.0775	0.0783
(0 2 0)	0.705	2.32×10^{-2}	0.0867	0.0878
(1 0 0)	0.750	3.83×10^{-2}	0.0940	0.0943
(0 1 1)	0.835	1.08×10^{-2}	0.108	0.108
(1 −1 1)	0.895	5.00×10^{-3}	0.117	0.115
(0 0 2)	0.935	6.88×10^{-3}	0.123	0.129
(0 3 0)	0.990	1.24×10^{-2}	0.132	0.132
(1 1 0)	1.025	3.05×10^{-2}	0.137	0.138
(2 −1 0)	1.080	3.68×10^{-3}	0.145	0.145
(0 2 1)	1.125	5.28×10^{-3}	0.152	0.152
(1 0 1)	1.175	3.48×10^{-2}	0.159	0.159
(2 1 −1)	1.210	6.60×10^{-3}	0.165	0.165
(0 1 2)	1.275	2.43×10^{-3}	0.174	0.173
(1 2 0)	1.320	1.53×10^{-3}	0.181	0.182
(2 0 0)	1.370	1.58×10^{-3}	0.188	0.189
(0 0 3)	1.405	6.40×10^{-4}	0.194	0.193
(1 1 1)	1.460	1.82×10^{-3}	0.202	0.203
(2 −1 1)	1.515	4.20×10^{-4}	0.210	0.209
(1 0 2)	1.615	2.50×10^{-4}	0.224	0.223
(1 2 1)	1.760	1.00×10^{-4}	0.245	0.247
(2 0 1)	1.815	1.40×10^{-4}	0.253	0.253
(2 1 1)	2.110	3.60×10^{-4}	0.296	0.297

[This article is copyrighted as indicated in the article. Reuse of AIP content is subject to the terms at: http://scitation.aip.org/termsconditions. Downloaded to] IP: 202.119.48.169 On: Wed, 22 Apr 2015 12:22:17

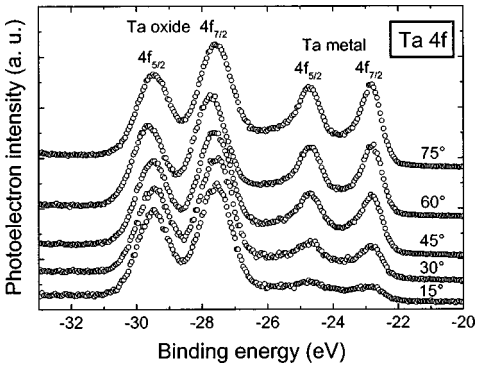

FIG. 6. Angle-resolved XPS spectra for Ta, indicating a mixture of metallic and oxidized Ta near the surface. The peaks corresponding to metallic Ta are strongly suppressed at low take-off angles.

oxidized state of Ta. The measurements at different take-off angles point to substantial oxidation of the capping layer at all accessible sampling depths (which are on the order of three times the inelastic mean-free paths for photoelectrons[30]). By contrast, the peaks associated with metallic Ta show a distinct depth dependence indicating almost exclusively oxidized states near the surface. The angle-resolved Al $2p$ spectra in Fig. 7 give a very similar picture for the distribution of metallic and oxidized Al; in particular, these spectra provide direct evidence for the extensive diffusion of Al into the capping layer.

Assuming an inelastic mean free path of ~25 Å for the Al $2p$ and Ta $4f$ photoelectrons, we can estimate the oxide thickness from the ratio of the integrated intensities of the oxide and metal peaks at different angles.[30] This method gives an oxide thickness of about 30 Å both for the Al and the Ta data, which compares favorably with the thickness of 26 ± 10 Å determined by x-ray reflectivity. In addition, the integrated peak intensities indicate a ratio of Ta to Al atoms of about 1:2 at the surface, which was also corroborated by supplementary Auger electron measurements.

V. DISCUSSION

The oxidation of Ta surfaces and capping layers has also been reported by other groups[8,31] and is consistent with the above analysis, indicating that the Ta capping layer has been transformed into an oxide layer which contains a mixture of Ta oxide and Al oxide. With Al as the prevailing atomic species near the surface, a relatively light oxide layer should develop, which is in agreement with the low density of the topmost layer in Table II obtained from x-ray reflectivity. However, the extremely low density of 2 ± 1 g/cm^3 indicates most probably a loosely packed or porous oxide which is not uncommon for natural oxide layers formed in air.[32] The increasing simultaneous presence of metallic Ta and Al with depth suggests that below the oxide layer Ta and Al coexist in metallic form in the same film, which further corroborates the formation of interdiffusion layers assumed in our structural model.

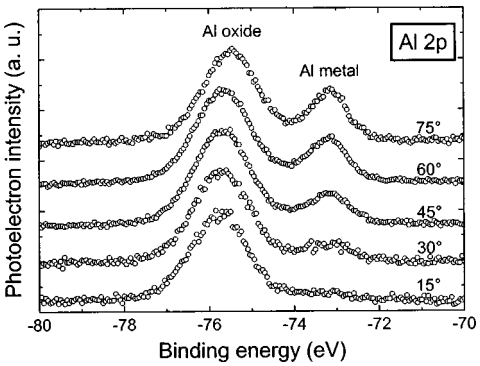

FIG. 7. Angle-resolved XPS spectra for Al, showing the presence of metallic and oxidized Al near the surface with a depth dependence similar to Ta.

In view of the previous study on the same sample, it is evident that the multilayer diffraction pattern has changed drastically over time. The reflectivity data taken shortly after growth still show diffraction peaks which are on the same intensity scale for incident angles between 0.5° and 2.5°, in agreement with the theoretical spectrum in Fig. 2. This feature is no longer present in the data measured after 41 months, which exhibit peak reflectivities dropping by decades in the same angular range (Fig. 3). Although a numerical comparison is difficult because the data in Ref. 16 have not been converted to absolute reflectivities, there can be no doubt about the severe ageing of the Ta/Al multilayer.

How reasonable is it to explain the observed degradation by interdiffusion at room temperature? The time needed to homogenize the bilayers can be assessed from the characteristic diffusion length

$$l=\sqrt{Dt}$$

with

$$D=D_0\exp(-Q/RT), \tag{11}$$

where D is the diffusion coefficient with activation energy Q, $R=8.314\,\mathrm{J\,mol^{-1}\,K^{-1}}$ is the gas constant, T denotes the absolute temperature, and t is time. We are not aware of interdiffusion coefficients for the Ta/Al system; however, we can evaluate the time associated with $l=20$ Å for favorable conditions, exemplified here by fcc Al with a relatively low activation energy of $Q=142.0$ kJ/mol and $D_0=1.7$ cm^2/s for substitutional self-diffusion.[33] The resulting time scale for diffusion at $T=300$ K is still three orders of magnitude too large to account for the experimental observations. On the other hand, it must be emphasized that the dominant diffusion mechanism at low temperatures frequently involves diffusion along defects, leading to effective diffusion coefficients which can be substantially higher than those for lattice diffusion alone. In particular, relatively open structures like grain boundaries can become important high-diffusivity paths at low temperatures with significantly reduced activation energies.[34] In fact, a rough calculation shows that activation energies of ~120–130 kJ/mol are sufficient to yield room temperature diffusion lengths of a few 10 Å within several months to years. Since in general sputter deposition does not produce highly perfect crystalline layers, it is very likely that the multilayer building blocks have been grown with a considerable amount of lattice defects. For the particular sample under investigation, the existence of grain boundaries is explicitly known from the observation of tex-

[This article is copyrighted as indicated in the article. Reuse of AIP content is subject to the terms at: http://scitation.aip.org/termsconditions. Downloaded to] IP: 202.119.48.169 On: Wed, 22 Apr 2015 12:22:17

ture in the high-angle diffraction data measured shortly after growth. Grain boundary diffusion has also been identified as an important factor for the interdiffusion kinetics of Ta/Ni-based multilayers.[9]

We conclude that bilayer interdiffusion should be considered as a realistic degradation mechanism here in spite of the relatively low temperature. Moreover, it seems possible that the extended interfaces which have been reported for Ta/Al superlattices[35] represent nothing more than the initial stage of the process depicted in Fig. 4, when the mutual interdiffusion of Ta and Al still involves only a few atomic layers.

Since growth-induced defects appear to be important, the stability of Ta/Al multilayers might be expected to depend largely on the details of the deposition process. However, there might also be an *intrinsic* lack of stability in Ta/Al multilayers. Lyubimov *et al.* have put forward this conjecture in a brief technical note, where they report the substantial disintegration of Ta/Al superlattices which were kept in a sealed container at room temperature for 6 months.[15] Their samples were produced by magnetron sputtering with bilayer thicknesses between 45 and 65 Å. The initially strong Bragg peaks, resulting from the deposition of ~100 periods, had disappeared except for the first order maximum, which however was found reduced in intensity by a factor of 10. This behavior, observed for six samples on glass and Si substrates, was attributed to diffusion rather than chemical transformation. Little thermal stability was also reported in another study,[13] where superlattices were annealed for 2 h at various temperatures between 200 and 1000 °C. Considerably reduced peak reflectivities were already observed at low annealing temperatures, preceding the complete disappearance of the original diffraction pattern at 600 °C because of a solid state reaction. It should also be pointed out that the strong intermixing of Ta/Al bilayers could be connected with the potential enhancement of interdiffusion coefficients for films on the nanometer scale, which are known to depend explicitly on the film thicknesses and concentration gradients.[5,6] Clearly, further work is needed to clarify the issue of ageing in this material system.

The observation of correlated interface roughness can only be related to the growth process, which inevitably results in nonideal interfaces with spatial Fourier components that typically propagate in the growth direction during the deposition of subsequent layers. In fact, interfacial transition layer widths of up to 10 Å have been found in Ta/Al superlattices produced under similar conditions.[12] Whereas the correlation of roughness on short wavelengths is strongly affected by diffusion, this is much less important for long length scales,[36] which should therefore mainly contribute to the diffuse reflectivity pattern in Fig. 3.

VI. CONCLUSIONS

The apparent lack of thermal stability renders Ta/Al multilayers unsuitable for x-ray monochromator applications in spite of their good reflection properties; exposing such multilayers to white synchrotron radiation will almost certainly result in rapid disintegration due to the intense heat load. Further investigations are necessary to determine whether the observed instability is intrinsic to the material system or essentially related to defects from the deposition process. Nevertheless, the attractive properties of Ta/Al multilayers might still be used in x-ray optics if the bilayers could be made from modified, Ta/Al-based materials with enhanced stability that essentially maintain the x-ray contrast. For example, the thermal stability of Co/C multilayers has been considerably improved by substantial doping with N;[6] alternatively, spacer materials with strong chemical bonds can be employed yielding, for instance, excellent high-temperature stability in Pt/Al_2O_3 multilayers[37] (however, an appreciable solid state reaction was found for Co/Al_2O_3[38]).

Since Fibonacci-type multilayers have advantages for x-ray monochromator applications (cf. Sec. II), the properties of their diffraction spectra are also of direct importance and not only a tool for structural analysis. It is interesting to note that the diffraction spectrum of the strongly interdiffused sample still shows all characteristics of a 3CF pattern (cf. Table III). We conclude that the mere persistence of a 3CF quasiperiodic diffraction spectrum despite the severe bilayer disintegration points to an astonishing *stability of quasiperiodic diffraction patterns against disorder*. This observation, far from obvious in the absence of translational symmetry, is in accordance with findings of Todd *et al.* that the presence of growth-induced disorder does not seem to seriously disturb the quasiperiodic properties of a GaAs/AlAs Fibonacci multilayer.[39] Such robustness against random as well as systematic imperfections might prove very helpful for the successful realization of tailored quasiperiodic multilayers for specific applications. It should also be noted that systematic deviations from the intended layer thicknesses (e.g., due to calibration errors) do *not* affect the quasiperiodicity, since $d_B/d_A \neq \xi$ or $d_C/d_A \neq \eta$ still lead to quasiperiodic ordering due to topologically equivalent three-dimensional parent lattices.[16]

Finally, we would like to emphasize that the number of Fibonacci generations resulting in the highest experimental peak reflectivities might be significantly smaller than intuitively expected. Obviously, an upper limit of useful layers is set by the x-ray penetration depth, which is limited by absorption and can therefore be relatively small due to the use of high-Z materials. For the 3CF sequence studied here, the (2 1 1) peak reflectivity saturates under ideal conditions after 12 Fibonacci generations as shown in Fig. 8. However, peak reflectivities of real multilayers depend crucially on the extent of interface roughness, which affects in particular the interesting peaks at higher q values. If the common phenomenon of kinetic roughening occurs during sample growth, the resulting peak reflectivities will be determined by a competition between the number of contributing interfaces and the corresponding increase in interface roughness. It is well known that the rms roughness σ on top of a single, growing layer increases with deposition time t according to a power law $\sigma \propto t^{\beta}$ due to the intrinsic fluctuations of the deposition process.[40] As the number of layers increases strongly for higher Fibonacci generations (cf. Fig. 8), quite large interface roughnesses can, in principle, arise from this mecha-

[This article is copyrighted as indicated in the article. Reuse of AIP content is subject to the terms at: http://scitation.aip.org/termsconditions. Downloaded to] IP: 202.119.48.169 On: Wed, 22 Apr 2015 12:22:17

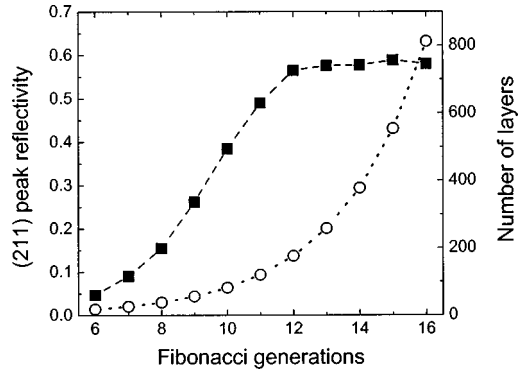

FIG. 8. Theoretical (2 1 1) peak reflectivity for the sample structure from Fig. 1 as a function of Fibonacci generations (squares). Open circles correspond to the total number of layers in the sample.

nism, and it is possible that the experimental peak reflectivities will drop considerably if a certain number of generations is exceeded. However, when different materials are deposited alternatively, typically a more complex behavior than the above power law is observed, since the height fluctuations of the dynamical growth front need not agree with the roughness of the later buried interface if wetting phenomena give rise to smoothing effects.[41] Therefore the optimal number of Fibonacci generations should be determined empirically.

ACKNOWLEDGMENTS

One of the authors (P.Y.) wishes to thank the Alexander von Humboldt foundation and the University Sains Malaysia for research fellowships. They are indebted to Dr. T. H. Metzger for experimental advice and to Professor W. Moritz and Dr. Li Xingzhong for helpful discussions, and to Dr. N. Tamura for a critical reading of the manuscript.

[1] D. B. McWhan, in *Synthetic Modulated Structures*, edited by L. L. Chang and B. C. Giessen (Academic, New York, 1985).
[2] E. Spiller, in *Physics, Fabrication and Applications of Multilayered Structures*, edited by P. Dhez and C. Weisbuch (Plenum, New York, 1987).
[3] N. N. Salashchenko, S. S. Andreev, Y. Y. Platonov, E. A. Shamov, S. Y. Zuev, and A. I. Chumakov, Surf. Investigation **12**, 269 (1997).
[4] B. X. Liu, O. Jin, and Y. Ye, J. Phys.: Condens. Matter **8**, L79 (1996).
[5] A. L. Greer and F. Spaepen, in *Synthetic Modulated Structures*, edited by L. L. Chang and B. C. Giessen (Academic, New York, 1985).
[6] H. L. Bai, E. Y. Jiang, and C. D. Wang, Thin Solid Films **304**, 278 (1997).
[7] T. Kobayashi, H. Nakamura, and R. Nakatani, J. Appl. Phys. **69**, 8285 (1991); M. Naoe and S. Nakagawa, *ibid.* **79**, 5015 (1996).
[8] T. C. Huang, J. P. Nozieres, V. S. Speriosu, H. Lefakis, and B. A. Gurney, Appl. Phys. Lett. **60**, 1573 (1992).
[9] I. Hashim, H. A. Atwater, K. T. Y. Kung, and R. M. Valletta, J. Appl. Phys. **74**, 458 (1993).
[10] H. van Leuken, A. Lodder, and R. A. de Groot, J. Phys.: Condens. Matter **3**, 3945 (1991).
[11] S. Morohashi, K. Gotoh, and S. Komiya, Appl. Phys. Lett. **64**, 785 (1994).
[12] S. S. Jiang, A. Hu, H. Chen, W. Liu, Y. X. Zhang, Y. Qiu, and D. Feng, J. Appl. Phys. **66**, 5258 (1989).
[13] A. Hu, S. S. Jiang, H. Chen, W. Liu, Y. Qiu, and D. Feng, Phys. Status Solidi A **117**, 221 (1990).
[14] R. W. Peng, A. Hu, and S. S. Jiang, Appl. Phys. Lett. **59**, 2512 (1991).
[15] A. G. Lyubimov, Y. Kshyan-Yang, A. S. Ilyushin, and U. Dzi-Tsin, Sov. Tech. Phys. Lett. **17**, 211 (1991).
[16] R. W. Peng, A. Hu, S. S. Jiang, C. S. Zhang, and D. Feng, Phys. Rev. B **46**, 7816 (1992).
[17] S. S. Jiang, R. W. Peng, A. Hu, J. Zou, D. J. H. Cockayne, and A. Sikorski, J. Appl. Crystallogr. **30**, 114 (1997).
[18] M. Kohmoto, L. P. Kadanoff, and C. Tang, Phys. Rev. Lett. **50**, 1870 (1983); M. Kohmoto, B. Sutherland, and C. Tang, Phys. Rev. B **35**, 1020 (1986); R. Merlin, IEEE J. Quantum Electron. **24**, 1791 (1988); K. Hirose, D. Y. K. Ko, and H. Kamimura, J. Phys.: Condens. Matter **4**, 5947 (1992); N. Sun, D. Hennig, M. I. Molina, and G. P. Tsironis, *ibid.* **6**, 7741 (1994); P. Tong, Phys. Rev. B **52**, 16301 (1995).
[19] R. Merlin, K. Bajema, F.-Y. Juang, and P. K. Bhattacharya, Phys. Rev. Lett. **55**, 1768 (1985).
[20] B. W. Batterman and D. H. Bilderback, in *Handbook on Synchrotron Radiation*, edited by G. S. Brown and D. E. Moncton (North-Holland, Amsterdam, 1991, Vol. 3); J. B. Kortright, J. Magn. Magn. Mater. **156**, 271 (1996), and references therein.
[21] J. Birch, M. Severin, U. Wahlström, Y. Yamamoto, G. Radnoczi, R. Riklund, and J.-E. Sundgren, Phys. Rev. B **41**, 10398 (1990).
[22] Z. C. Chen, R. Savit, and R. Merlin, Phys. Rev. B **37**, 4375 (1988); F. Axel and H. Terauchi, Phys. Rev. Lett. **66**, 2223 (1991).
[23] A. Hu, Z. X. Wen, S. S. Jiang, W. T. Tong, R. W. Peng, and D. Feng, Phys. Rev. B **48**, 829 (1993).
[24] R. W. James, *The Optical Principles of the Diffraction of X-rays* (Ox Bow, Woodbridge, CT, 1962).
[25] L. G. Parratt, Phys. Rev. **95**, 359 (1954).
[26] F. Stanglmeier, B. Lengeler, W. Weber, H. Göbel, and M. Schuster, Acta Crystallogr., Sect. A: Found. Crystallogr. **48**, 626 (1992).
[27] L. Névot and P. Croce, Rev. Phys. Appl. **15**, 761 (1980).
[28] D. E. Savage, J. Kleiner, N. Schimke, Y.-H. Phang, T. Jankowski, J. Jacobs, R. Kariotis, and M. G. Lagally, J. Appl. Phys. **69**, 1411 (1991); T. Salditt, T. H. Metzger, and J. Peisl, Phys. Rev. Lett. **73**, 2228 (1994).
[29] The packing densities are 0.13 atoms/Å^2 for Ta on bcc (110) planes and 0.14 atoms/Å^2 for Al on fcc (111) planes.
[30] D. Briggs and M. P. Seah, *Practical Surface Analysis*, 2nd ed. (Wiley, London, 1983), Vol. 1.
[31] H. L. Meyerheim, B. Lengeler, and H. E. Göbel, J. Appl. Phys. **68**, 2694 (1990).
[32] A. Plech, U. Klemradt, H. Metzger, and J. Peisl, J. Phys.: Condens. Matter **10**, 971 (1998).
[33] A. M. Brown and M. F. Ashby, Acta Metall. **28**, 1085 (1980).
[34] D. A. Porter and K. E. Easterling, *Phase Transformations in Metals and Alloys*, 2nd ed. (Chapman & Hall, London, 1992), Chap. 2.
[35] G. Carlotti, G. Socino, A. Hu, H. Xia, and S. S. Jiang, J. Appl. Phys. **75**, 3081 (1994).
[36] D. G. Stearns, J. Appl. Phys. **71**, 4286 (1992).
[37] C. Morawe and H. Zabel, Appl. Phys. Lett. **67**, 2612 (1995).
[38] C. Morawe and H. Zabel, J. Appl. Phys. **77**, 1969 (1995).
[39] J. Todd, R. Merlin, R. Clarke, K. M. Mohanty, and J. D. Axe, Phys. Rev. Lett. **57**, 1157 (1986).
[40] For an overview see: J. Krug, Adv. Phys. **46**, 139 (1997).
[41] U. Klemradt, M. Funke, M. Fromm, B. Lengeler, J. Peisl, and A. Förster, Physica B **221**, 27 (1996).

[This article is copyrighted as indicated in the article. Reuse of AIP content is subject to the terms at: http://scitation.aip.org/termsconditions. Downloaded to] IP: 202.119.48.169 On: Wed, 22 Apr 2015 12:22:17